HHS Public Access

Author manuscript

Biochem J. Author manuscript; available in PMC 2015 October 29.

Published in final edited form as:

Biochem J. 2014 August 1; 461(3): 487–495. doi:10.1042/BJ20140337.

TMPRSS13 deficiency impairs stratum corneum formation and epidermal barrier acquisition

Daniel H. Madsen, **Roman Szabo**, **Alfredo A. Molinolo**, and **Thomas H. Bugge**

Oral and Pharyngeal Cancer Branch, National Institute of Dental and Craniofacial Research, National Institutes of Health, Bethesda, MD 20892

Abstract

Membrane-anchored serine proteases serve as important regulators of multiple developmental and homeostatic processes in mammals. Transmembrane protease, serine 13, TMPRSS13 (also known as mosaic serine protease large-form, MSPL), is a membrane-anchored serine protease with unknown biological functions. In this study, we used mice with the *Tmprss13* gene disrupted by a β-galactosidase-neomycin fusion gene insertion to study the expression and function of the membrane-anchored serine protease. High levels of *Tmprss13* expression were found in the epithelia of the oral cavity, upper digestive tract, and skin. Compatible with this expression pattern, *Tmprss13*-deficient mice displayed abnormal skin development leading to a compromised barrier function, as measured by trans-epidermal fluid loss rate of newborn mice. The study provides the first biological function for the transmembrane serine protease, TMPRSS13.

Keywords

type II transmembrane serine protease; mouse gene targeting; mosaic serine protease large-form; MSPL; transmembrane protease serine 13; skin development

INTRODUCTION

The membrane-anchored serine proteases are a large family of trypsin-like serine proteases that emerged at the turn of the millennium in large part through the mining of the recently available genome and expressed sequence tag databases. This family constitutes 20 members in humans, and it includes the type I transmembrane serine protease, tryptase γ1, the glycophophoinositol-anchored serine proteases, prostasin and testisin, and the type II transmembrane serine proteases, human airway trypsin-like protease (HAT), downregulated in squamous cell carcinoma (DESC)1, transmembrane protease, serine (TMPRSS)11A, HAT-like 4, HAT-like 5, hepsin, TMPRSS2, TMPRSS3, TMPRSS4, TMPRSS13/mosaic serine protease large-form (MSPL), enteropeptidase, matriptase, matriptase-2, matriptase-3,

Address correspondence and reprint requests to: Thomas H. Bugge, Ph.D., Proteases and Tissue Remodeling Section, Oral and Pharyngeal Cancer Branch, National Institute of Dental and Craniofacial Research, National Institutes of Health, 30 Convent Drive, Room 211, Bethesda, MD 20892, Phone: (301) 435-1840, Fax: (301) 402-0823, thomas.bugge@nih.gov.

Author contributions

Daniel H. Madsen,Roman Szabo, and Alfredo A. Molinolo performed the experiments. Daniel H. Madsen and Thomas H. Bugge conceived the study and wrote the manuscript.

polyserase-1, and corin (reviewed in [1-3]). Human genetics and loss of function studies in mice have revealed important and surprisingly diverse roles of membrane-anchored serine proteases in mammalian development and postnatal homeostasis. These include placental morphogenesis [4, 5], neural tube closure [6], epithelial tight junction formation [7, 8], auditory and vestibular hair cell survival [9, 10], apical epithelial sodium entry [11], blood pressure [12, 13], iron homeostasis [14-16], male fertility [17, 18], and skin development.

Transmembrane protease serine 13 (TMPRSS13), also known as mosaic serine protease large-form (MSPL), is a member of the hepsin/TMPRSS subfamily of type II transmembrane serine proteases [3, 19]. TMPRSS13 is a functional protease that is capable of cleaving macromolecular substrates and can be inhibited by serine protease inhibitors of the Kunitz-type [20]. As a first step towards defining the biological functions of TMPRSS13, we herein conducted a detailed analysis of the expression of the mouse *Tmprss13* gene and determined the consequences of *Tmprss13* deficiency in mice. We report that *Tmprss13* is highly expressed in stratified squamous epithelium, and that *Tmprss13* display a defect in skin development. The study provides the first biological function for the transmembrane serine protease, TMPRSS13

MATERIALS AND METHODS

Mice

All experiments were performed in an Association for Assessment and Accreditation of Laboratory Animal Care International-accredited vivarium following Institutional Guidelines and standard operating procedures. Mice carrying a targeted *Tmprss13* allele (*Tmprss13*^{tm1Dgen}/J) were generated by Deltagen Inc. (San Mateo, CA) and acquired from the Jackson Laboratories via the Deltagen and Lexicon Trans-NIH Mouse Initiative. Gene targeting was performed by homologous recombination in 129P2/OlaHsd-derived E14 embryonic stem cells. The targeting vector contained a promoterless LacZ-Neo fusion gene (β-galactosidase reporter) and recombination resulted in the deletion of a 4 kb region of the *Tmprss13* gene. This deleted region includes the last 92 bp of exon 9, which includes the catalytic aspartic acid reside, and the entire exon 10. The in-frame insertion of the LacZ-Neo fusion gene leads to the expression of a fusion protein consisting of the first 377 amino acids of TMPRSS13 fused to β-galactosidase. Genotyping was performed using the following primer sets: moIMR0012 (5'-GGGTGGGATTAGATAAATGCCTGCTCT-3'), oIMR6316 (5'-AAATGACCCACCTAATTAGCTGTAG-3'), and oIMR6318 (5'-GCCTCAATGAGACCTGTTGGATCAC-3'). All *Tmprss13*$^{-/-}$ and *Tmprss13*$^{+/+}$ littermate controls used in the study were offspring of intercrossed *Tmprss13*$^{+/-}$ mice on a 129P2/OlaHsd(50%)/C57BL6/J(50%) background. The transepidermal fluid loss assay was performed exactly as described [21]. In brief, newborn pups were separated from their mother to prevent fluid intake and placed in a 37°C incubator. The rate of epithelial fluid loss was estimated by measuring the reduction of body weight of the individual pups as a function of time over a period of 6 h.

RT-PCR analysis

Skin was collected from newborn mice and epidermis was separated from dermis after heating the skin at 50°C in PBS with 10 mM EDTA. The epidermis was homogenized in Trizol reagent (Life Technologies, Grand Island, NY) using a glass homogenizer and total RNA was prepared according to the manufacturer's recommendations. Reverse transcription was performed using the Ambion RETROscript kit (Life Technologies) according to the manufacturer's instructions. First strand cDNA synthesis was performed using an oligo $(dT)_{18}$ primer. Subsequent PCR amplification was performed using JumpStart REDtaq ReadyMix (Sigma-Aldrich, St. Louis, MO) with the primer pairs indicated in Table 1.

Histological and blood chemistry analysis

Newborn pups were euthanized by decapitation and fixed for 24 h in zinc-buffered formalin (Anatech Ltd., Battle Creek, MI). Tissues from adult mice were collected and fixed for 24 h in zinc-buffered formalin. Newborn pups and tissues from adult mice were embedded in paraffin, sectioned, stained with hematoxylin and eosin (H&E) digitally scanned using an Aperio Scanscope, and analyzed using Aperio Imagescope software. Epidermal and stratum corneum thickness of newborn mice were determined on a region-matched 1 cm area of dorsal skin performing 100 measurements for each mouse. For a cohort of 12 months old *Tmprss13*$^{-/-}$ and littermate *Tmprss13*$^{+/+}$ and *Tmprss13*$^{+/-}$ mice, blood was collected and serum was submitted to the NIH Clinical Center Department of Laboratory Medicine (Bethesda, MD) for blood chemistry analysis.

X-gal staining

Embryos at embryonic day 14.5, 15.5 and 16.5 were extracted, and organs from adult mice were excised and sliced. Tissue and embryos were placed in buffered zinc formalin for 15 min, washed thoroughly in PBS and stained overnight at 37°C with a β-galactosidase staining kit (Roche, Indianapolis, IN). The tissues were post-fixed for 16 h in zinc-buffered formalin and embryos were photographed using a Canon EOS Rebel SL1 camera (Canon Inc., Melville, NY). The X-gal-stained tissues thereafter were embedded in paraffin and sectioned. Sections were counter-stained with nuclear fast red or hematoxylin and subsequently examined for *Tmprss13* expression.

Immunohistochemistry

Tissue sections of X-gal stained, PFA-fixed tissues were prepared as described above or generated from tissues fixed for 24 h in PFA prior to embedding. Antigens were retrieved by incubation for 10 min at 37°C with 10 μg/ml proteinase K (Fermentas, Hanover, MD). Immunohistochemistry was performed using a polyclonal rabbit anti-keratin 5 antibody (Covance Inc., Princeton, NJ) diluted 1 to 5000 in PBS with 2% BSA, polyclonal rabbit anti-keratin 10 (Covance Inc.) diluted 1 to 2000 in PBS with 2% BSA or polyclonal rabbit anti-profilaggrin/filaggrin antibody (Covance Inc.) diluted 1 to 2000 in PBS with 2% BSA. After washing the slides with PBS, bound antibodies were visualized using biotin-conjugated anti-rabbit secondary antibody (Vector Laboratories, Burlingame, CA) and a Vectastain ABC kit (Vector Laboratories). SIGMA*FAST* 3,3'-diaminobenzidine was used as the substrate

(Sigma-Aldrich). Stained slides were digitally scanned using an Aperio Scanscope and analyzed using Aperio Imagescope software.

Profilaggrin processing assays

Epidermis from newborn mice was isolated as decribed above and homogenized in 50 mM Tris/HCl, pH 8.0, 10 mM EDTA, and 8 M urea. Homogenates were clarified by centrifugation at 20,000 × g, 4°C, 30 min. Samples were mixed with 4 × LDS NuPAGE sample buffer (Life Technologies) containing 1 M β-mercaptoethanol, boiled for 5 min, and separated on 4-12% Bis-Tris NuPAGE gels. Proteins on the gels were either stained with Coomassie brilliant blue or transferred to 0.2 μm pore size PVDF membranes (Life Technologies). Membranes were blocked with 5% nonfat dry milk in Tris-buffered saline containing 0.05% Tween-20 (TBS-T) for 1 h at room temperature, and then probed overnight at 4°C with a polyclonal rabbit anti-profilaggrin/filaggrin antibody (Covance Inc.) diluted 1 to 3000 in 5% milk in TBS-T or a rabbit anti-GAPDH antibody (Cell Signaling Technology Inc., Danvers, MA) diluted 1 to 3000 in 5% milk in TBS-T. The next day, the membrane was washed 4 × 5 min with TBS-T and incubated for 1 h with alkaline phosphatase-conjugated secondary anti-rabbit antibody (DAKO, Carpinteria, CA). After 4 × 5 min washes with TBS-T, the membrane was developed using nitro blue tetrazolium/5-Bromo-4-chloro-3-indolyl phosphate solution (Pierce, Rockford, IL).

Epidermal tight junction assay

Epidermal tight junction integrity was determined as described previously [8, 22] Newborn mice were injected with 50 μl of 10 mg/ml EZ-LinkTM Sulfo-NHS-LC-Biotin (Thermo Fisher Scientific Inc., Waltham, MA) in PBS containing 1 mM $CaCl_2$ into the interscapular region of the dermis. Mice were euthanized by decapitation 30 min later and the skin was excised and embedded in OCT. Five μm frozen sections were fixed in 95% ethanol at 4°C for 30 min and in 100% acetone at room temperature for 1 min. Sections were blocked for 30 min with 2% BSA in PBS, incubated with ZO-1 rabbit polyclonal antibody (ZYMED Laboratories, South San Francisco, CA, diluted 1:50 in blocking solution) on at 4 °C, then washed three times with PBS and incubated for 60 min at room temperature with a mixture of Alexa Fluor 594 conjugated goat anti-rabbit IgG (Life Technologies, diluted 1:400 in blocking solution) and streptavidin Alexa Fluor 488 conjugate (Life Technologies, 5 μg/ml in blocking solution). Sections were washed three times with PBS and mounted with VectaShield HardSet Mounting Medium with DAPI (Vector Laboratories).

RESULTS

Tmprss13 is expressed at high levels in stratified squamous epithelium

To obtain information about the expression of *Tmprss13*, we took advantage of a mouse strain that carries a promoterless *LacZ-neomycin* fusion gene inserted into the endogenoeus *Tmprss13* locus by homologous recombination in embryonic stem cells (Figure 1A, hereafter termed *Tmprss13*$^{+/-}$ mice). This insertion causes the synthesis of a tripartite TMPRSS13-β-galactosidase-neomycin fusion protein in cells actively transcribing *Tmprss13* (Figure 1B), and therefore provides a convenient means to detect the expression of the gene by *in situ* staining using the chromogenic β-galactosidase substrate, X-gal, followed by

histological sectioning of stained sections. Staining of organs from young adult *Tmprss13*$^{+/-}$ mice showed particularly strong expression of the membrane-anchored serine protease in multi-layered squamous epithelium. This included the epidermis, hair follicles, oral epithelium, cornea, and the upper digestive tract (Figure 2A-I and Table 2). Transitional epithelium of the bladder also expressed *Tmprss13* at high levels (Figure 2J), while the protease was expressed at much lower levels in prostate, heart, intestine, kidney, and thymus (Figure 2K and L, Table 2, and data not shown). The specificity of staining in all cases was verified by the absence of staining in wildtype littermates. *Tmprss13* expression in squamous epithelium was strictly suprabasal, as shown by combining X-gal staining with staining for the basal keratinocyte marker, keratin 5 (Figure 3A and B). Similar double stainings with antibodies against keratin 10 and profilaggrin/filaggrin revealed that *Tmprss13* is expressed in both the spinous and granular/transitional layer of the epidermis (Figure 3C and D). The onset of *Tmprss13* expression in the developing epidermis was determined by X-gal staining of embryos from embryonic day (E)14.5, E15.5, and E16.5 (Figure 3E). Weak *Tmprss13* expression was evident in the facial region, developing ear, and limbs at E14.5. *Tmprss13* expression was more intense in these areas at E15.5 and a larger part of the developing epidermis expressed the protease, while at E16.5 the entire developing epidermis expressed *Tmprss13* at a high level. The embryonic expression of *Tmprss13* was also suprabasal, as judged by histological analysis of X-gal stained embryos (Figure 3F-I).

Tmprss13-deficient mice have abnormal skin development

The above studies revealed that *Tmprss13* is highly expressed in suprabasal layers of the epidermis and oral cavity. Because several membrane-anchored serine proteases and their cognate inhibitors display a similar expression pattern and have previously been shown to be essential for skin development [21, 23-26], we next investigated the role of TMPRSS13 in these processes. For this purpose, we interbred *Tmprss13*$^{+/-}$ mice to generate *Tmprss13*$^{-/-}$ and associated wildtype littermate control mice. In H&E-stained sections, the stratum corneum of normal epidermis display a characteristic “basket weave” pattern with empty intercorneocyte lacunae (due to the extraction of the resident epidermal lipids during tissue processing) formed by a meshwork of interlocking flattened layers of corneocytes connected by desmosomes [27]. Interestingly, microscopic analysis of skin sections from newborn mice revealed that the stratum corneum of *Tmprss13*$^{-/-}$ epidermis was abnormally compacted, presenting with fewer and smaller intercorneocyte lacunae than their wildtype littermates (Figure 4, compare low magnification of epidermis in A and B and high magnification of stratum corneum in C and D). Indeed, a quantitative histomorphometric analysis revealed that the thickness of the stratum corneum of the *Tmprss13*$^{-/-}$ epidermis was reduced by 38 percent when compared to wildtype littermates (Figure 4E), while the thickness of the living (basal, spinous, and granular/transitional) layer of the epidermis did not differ between *Tmprss13*$^{-/-}$ and wildtype littermates (Figure 4F). To determine if the abnormal stratum corneum formation of *Tmprss13*$^{-/-}$ mice was associated with impaired epidermal barrier function, we next determined the trans-epidermal fluid loss rate in *Tmprss13*$^{-/-}$ and littermate control (*Tmprss13*$^{+/-}$ and *Tmprss13*$^{+/+}$) mice (Figure 4G). This analysis showed that loss of TMPRSS13, indeed, was associated with a 54 percent increase in the trans-epidermal fluid loss rate. Importantly, this difference could not be explained by

a general developmental delay, as the birth weight of *Tmprss13*$^{-/-}$ and littermate control mice did not differ (data not shown). The increased fluid loss through the *Tmprss13*$^{-/-}$ epidermis did not adversely affect postnatal survival under the applied experimental conditions, as revealed by the Mendelian representation of *Tmprss13*$^{-/-}$ mice in weaned offspring from *Tmprss13*$^{+/-}$ intercrosses (data not shown). Taken together, the above experiments demonstrate that TMPRSS13 contributes to stratum corneum formation and acquisition of the epidermal barrier.

To evaluate the long-term consequences of Tmprss13-deficiency, a histological examination of tissues from 7 and 12 months old *Tmprss13*$^{-/-}$ mice and littermate *Tmprss13*$^{+/+}$ or *Tmprss13*$^{+/-}$ mice was performed. All tissues included in table 2 were evaluated. No histological alterations were observed in the 7 month old mice (4 *Tmprss13*$^{-/-}$ mice and 3 littermate *Tmprss13*$^{+/+}$ or *Tmprss13*$^{+/-}$ mice). In the group of 12 months old mice (5 *Tmprss13*$^{-/-}$ mice and 6 littermate *Tmprss13*$^{+/+}$ or *Tmprss13*$^{+/-}$ mice) age-associated alterations were occasionally observed, but none of these appeared to be genotype specific. In addition, a blood chemistry analysis of protein levels of the following enzymes was performed: Alkaline Phosphatase, Alanine Aminotransferase, Aspartate Aminotransferase, Amylase, Creatine Kinase, and Lactate Dehydrogenase. Of these, Lactate Dehydrogenase was moderately elevated in the *Tmprss13*$^{-/-}$ mice compared to the littermate control mice, while other enzyme levels were normal (Supplementary Figure S1).

TMPRSS13-deficient mice display normal tight junction formation and profilaggrin processing

Proteolytic processing of the intracellular polyprotein, profilaggrin to filaggrin monomers is a hallmark of terminal epidermal differentiation. Although the actual cleavage of profilaggrin is executed by cytoplasmic cysteine calpains, profilaggrin processing is strictly dependent on the matriptase-prostasin cell surface proteolytic cascade, and filaggrin monomers are completely absent in mice deficient in either matriptase or prostasin [23, 24]. To gain mechanistic insights into how TMPRSS13 promotes stratum corneum formation, we next prepared urea/SDS extracts from the epidermis of newborn *Tmprss13*$^{-/-}$ and littermate control mice, as well as matriptase-deficient, *St14*$^{-/-}$ mice. As described previously [24], no filaggrin monomer was detected in extracts from matriptase-deficient epidermis when analyzed by SDS/PAGE followed by either Coomassie brilliant blue staining (Figure 5A, lane 1) or by Western blot with profilaggrin/filaggrin antibodies (Figure 5B, lane 1). Interestingly, however, profilaggrin processing was not affected by the loss of TMPRSS13, with the abundance of filaggrin monomer in the epidermis of *Tmprss13*$^{-/-}$ mice being indistinguishable from that of epidermis of littermate control mice (Figure 5A and B, compare lanes 2-5 with lanes 6-9).

Formation of epidermal tight junctions by granular layer keratinocytes is a second matriptase-prostasin cascade-dependent component of epidermal barrier formation [8, 23, 28]. To investigate if TMPRSS13 participates in epidermal tight junction formation, we next injected a reactive biotin tracer into the dermis of newborn matriptase-deficient (*St14*$^{-/-}$), *Tmprss13*$^{-/-}$, and wildtype littermates and followed the diffusion of the tracer through the epidermal layers by staining of frozen sections with Alexa Fluor 488-labeled streptavidin

(Figure 6). As described previously [8], the biotin tracer accumulated in the stratum corneum of matriptase-deficient epidermis (compare Figure 6A and B). However, no diffusion of the biotin tracer could be observed in TMPRSS13-deficient epidermis (compare Figure 6C and D). Taken together, these studies, unexpectedly, show that TMPRSS13 supports stratum corneum formation and epidermal barrier formation by a mechanism that is independent of both epidermal profilaggrin processing and epidermal tight junction formation.

TMPRSS13-deficient mice display delayed whisker growth

No abnormalities in pelage hair eruption or pelage hair appearance were noted in TMPRSS13-deficient mice (data not shown). However, the whiskers, which are fully erupted in mice at birth, appeared to be shorter in newborn TMPRSS13-deficient pups when compared to wildtype littermates (Figure 7A). Indeed, a morphometric analysis of whisker length at birth showed that loss of TMPRSS13 resulted in a 30% reduction of length of the whiskers (Figure 7B). This difference was transient with adult TMPRSS13-deficient mice displaying normal whiskers (data not shown).

DISCUSSION

We examined *Tmprss13* expression in the mouse and found that the gene encoding this relatively unexplored membrane-anchored serine protease was highly expressed in stratified keratinizing squamous epithelium of the epidermis, the oral cavity, and the squamous portion of upper digestive tract. HAT, DESC1, TMPRSS4, matriptase, and prostasin have all been shown previously to be expressed in the epidermis (reviewed in [1]), making this tissue remarkably rich in the expression of membrane-anchored serine proteases. By using stage-specific differentiation markers, *Tmprss13* expression could be localized to the spinous, granular, and transitional layers of the epidermis, while no expression in the proliferative basal compartment was observed. Compatible with this expression pattern, disruption of the *Tmprss13* gene caused a defect in epidermal barrier formation, as revealed by an incompletely developed stratum corneum and enhanced transepidermal fluid loss. The increased fluid loss did not affect postnatal or long-term survival, suggesting that TMPRSS13-deficient mice are capable of compensating for the increased transepidermal fluid loss by increased fluid intake. Compromised barrier function is most critical in the neonatal period, due to a high surface to volume ratio of neonates, a still poorly developed immune system, and the lack of pelage hair. It is, therefore, to be expected that barrier-compromised mice that survive the neonatal period also will be viable at later stages. Furthermore, the aberrant stratum corneum of the newborn mice was not observed in adult mice (not shown) and it is therefore plausible that also the skin barrier function is restored in adulthood.

This pattern of expression of *Tmprss13* in stratified squamous epithelium strikingly resembled that of matriptase and prostasin [23, 29, 30]. Furthermore, the defect in epidermal differentiation associated with TMPRSS13 deficiency was outwardly similar to that observed in matriptase and prostasin-deficient mice [23, 24]. Several lines of evidence provided in this study, however, suggest that TMPRSS13 acts either in parallel to the

matriptase-prostasin cascade, or that it acts downstream of the cascade, subsequent to an undefined cascade branch point. First, the defect in stratum corneum maturation and epidermal barrier function is less severe than that observed in matriptase- or prostasin-deficient mice, making it unlikely that TMPRSS13 acts upstream of the matriptase-prostasin cascade. Second, profilaggrin processing and epidermal tight junction formation, both of which are matriptase and prostasin-dependent processes, occur normally in TMPRSS13-deficient epidermis. The precise localization of TMPRSS13 relative to the matriptase-prostasin cascade, however, will have to await the development of antibodies of sufficient quality to detect TMPRSS13 in mouse epidermis.

The gene targeting strategy employed in this study allowed the amino terminal, non-catalytic, domains of TMPRSS13 to be expressed as part of a tripartite TMPRSS13-β-galactosidase-neomycin fusion protein. This raises the possibility that potential non-catalytic functions of TMPRSS13 may have been retained in the TMPRSS13-deficient mice, and that the retention of these non-catalytic functions may contribute to the relatively mild phenotype associated with the loss of this widely expressed protease. We find this to be unlikely, however, because all functions for stem domains of type II transmembrane serine proteases that have been elucidated to date are involved in regulating proteolytic functions, such as zymogen activation, substrate recognition, and inhibitor interactions [1-3].

Future studies will be aimed at uncovering the mechanistic basis of the epidermal barrier defect caused by loss of TMPRSS13. The epidermis of TMPRSS13-deficient mice displayed a seemingly normal capacity to form tight junctions and to process profilaggrin, although subtle impairments in either differentiation process cannot be excluded. This would suggest that TMPRSS13 could have a specific function in either epidermal lipid manufacturing or epidermal lipid extrusion [27]. If so, TMPRSS13 would substantially differ from matriptase and prostasin, which are essential for epidermal tight junction formation, profilaggrin processing, and epidermal lipid manufacturing.

In addition to impaired barrier formation, TMPRSS13-deficient mice displayed shorter whiskers at birth. This defect in hair follicle development could be a secondary response to the primary defects in interfollicular epidermal development described above. More likely, however, TMPRSS13-deficient mice present a primary defect in hair follicle development, because the membrane-anchored serine protease also was expressed at high levels in the hair follicle compartment.

Our analysis showed that *Tmprss13* is expressed to varying extent in a subset of non-stratified squamous epithelia and non-epithelial tissues. This includes high expression in transitional bladder epithelium, and low expression in prostate, cardiac muscle, intestine, kidney, and thymus. TMPRSS13-deficient mice in our colony were outwardly healthy when followed for up to 10 months, demonstrating that TMPRSS13 is dispensable for the life-sustaining function of these organs in the absence of external challenges or additional genetic deficits. Furthermore, no histological differences in *Tmprss13*-positive tissues between wildtype and *Tmprss13* knockout mice were observed, except for the aberrant stratum corneum of the epidermis.

In summary, our study provides the first biological function of TMPRSS13, and it identifies a third membrane-anchored serine protease important for epidermal development and acquisition of epidermal barrier function.

Supplementary Material

Refer to Web version on PubMed Central for supplementary material.

Acknowledgements

We thank Drs. Silvio Gutkind and Mary Jo Danton for critically reviewing this manuscript. Supported by the NIDCR Intramural Research Program. The authors declare no competing financial interests in relation to the work described.

REFERENCES

1. Bugge TH, Antalis TM, Wu Q. Type II transmembrane serine proteases. J. Biol. Chem. 2009; 284:23177–23181. [PubMed: 19487698]
2. Hooper JD, Clements JA, Quigley JP, Antalis TM. Type II transmembrane serine proteases. Insights into an emerging class of cell surface proteolytic enzymes. J. Biol. Chem. 2001; 276:857–860. [PubMed: 11060317]
3. Szabo R, Bugge TH. Membrane anchored serine proteases in cell and developmental biology. Annu. Rev. Cell Dev. Biol. 2011; 27
4. Hummler E, Dousse A, Rieder A, Stehle JC, Rubera I, Osterheld MC, Beermann F, Frateschi S, Charles RP. The channel-activating protease CAP1/Prss8 is required for placental labyrinth maturation. PLoS One. 2013; 8:e55796. [PubMed: 23405214]
5. Szabo R, Uzzun Sales K, Kosa P, Shylo NA, Godiksen S, Hansen KK, Friis S, Gutkind JS, Vogel LK, Hummler E, Camerer E, Bugge TH. Reduced prostasin (CAP1/PRSS8) activity eliminates HAI-1 and HAI-2 deficiency-associated developmental defects by preventing matriptase activation. PLoS Genet. 2012; 8:e1002937. [PubMed: 22952456]
6. Camerer E, Barker A, Duong DN, Ganesan R, Kataoka H, Cornelissen I, Darragh MR, Hussain A, Zheng YW, Srinivasan Y, Brown C, Xu SM, Regard JB, Lin CY, Craik CS, Kirchhofer D, Coughlin SR. Local protease signaling contributes to neural tube closure in the mouse embryo. Dev. Cell. 2010; 18:25–38. [PubMed: 20152175]
7. Buzza MS, Netzel-Arnett S, Shea-Donohue T, Zhao A, Lin CY, List K, Szabo R, Fasano A, Bugge TH, Antalis TM. Membrane-anchored serine protease matriptase regulates epithelial barrier formation and permeability in the intestine. Proc. Natl. Acad. Sci. U.S.A. 2010; 107:4200–4205. [PubMed: 20142489]
8. List K, Kosa P, Szabo R, Bey AL, Wang CB, Molinolo A, Bugge TH. Epithelial integrity is maintained by a matriptase-dependent proteolytic pathway. Am. J. Pathol. 2009; 175:1453–1463. [PubMed: 19717635]
9. Fasquelle L, Scott HS, Lenoir M, Wang J, Rebillard G, Gaboyard S, Francois F, Mausset-Bonnefont A-L, Neidhart E, Chabbert C, Puel JL, Guipponi M, B. D. Tmprss3, a transmembrane serine protease deficient in human DFNB8/10 deafness, is critical for Cochlear hair cell survival at the onset of hearing. J. Biol. Chem. 2010; 286:17383–17397. [PubMed: 21454591]
10. Scott HS, Kudoh J, Wattenhofer M, Shibuya K, Berry A, Chrast R, Guipponi M, Wang J, Kawasaki K, Asakawa S, Minoshima S, Younus F, Mehdi SQ, Radhakrishna U, Papasavvas MP, Gehrig C, Rossier C, Korostishevsky M, Gal A, Shimizu N, Bonne-Tamir B, Antonarakis SE. Insertion of beta-satellite repeats identifies a transmembrane protease causing both congenital and childhood onset autosomal recessive deafness. Nat. Genet. 2001; 27:59–63. [PubMed: 11137999]
11. Vallet V, Chraibi A, Gaeggeler HP, Horisberger JD, Rossier BC. An epithelial serine protease activates the amiloride-sensitive sodium channel. Nature. 1997; 389:607–610. [PubMed: 9335501]
12. Wu F, Yan W, Pan J, Morser J, Wu Q. Processing of pro-atrial natriuretic peptide by corin in cardiac myocytes. J. Biol. Chem. 2002; 277:16900–16905. [PubMed: 11884416]

13. Yan W, Wu F, Morser J, Wu Q. Corin, a transmembrane cardiac serine protease, acts as a pro-atrial natriuretic peptide-converting enzyme. Proc. Natl. Acad. Sci. U.S.A. 2000; 97:8525–8529. [PubMed: 10880574]
14. Du X, She E, Gelbart T, Truksa J, Lee P, Xia Y, Khovananth K, Mudd S, Mann N, Moresco EM, Beutler E, Beutler B. The serine protease TMPRSS6 is required to sense iron deficiency. Science. 2008; 320:1088–1092. [PubMed: 18451267]
15. Finberg KE, Heeney MM, Campagna DR, Aydinok Y, Pearson HA, Hartman KR, Mayo MM, Samuel SM, Strouse JJ, Markianos K, Andrews NC, Fleming MD. Mutations in TMPRSS6 cause iron-refractory iron deficiency anemia (IRIDA). Nat. Genet. 2008; 40:569–571. [PubMed: 18408718]
16. Folgueras AR, de Lara FM, Pendas AM, Garabaya C, Rodriguez F, Astudillo A, Bernal T, Cabanillas R, Lopez-Otin C, Velasco G. Membrane-bound serine protease matriptase-2 (Tmprss6) is an essential regulator of iron homeostasis. Blood. 2008; 112:2539–2545. [PubMed: 18523150]
17. Netzel-Arnett S, Bugge TH, Hess RA, Carnes K, Stringer BW, Scarman AL, Hooper JD, Tonks ID, Kay GF, Antalis TM. The glycosylphosphatidylinositol-anchored serine protease PRSS21 (testisin) imparts murine epididymal sperm cell maturation and fertilizing ability. Biol. Reprod. 2009; 81:921–932. [PubMed: 19571264]
18. Kawano N, Kang W, Yamashita M, Koga Y, Yamazaki T, Hata T, Miyado K, Baba T. Mice lacking two sperm serine proteases, ACR and PRSS21, are subfertile, but the mutant sperm are infertile in vitro. Biol. Reprod. 2010; 83:359–369. [PubMed: 20484738]
19. Kim DR, Sharmin S, Inoue M, Kido H. Cloning and expression of novel mosaic serine proteases with and without a transmembrane domain from human lung. Biochim. Biophys. Acta. 2001; 1518:204–209. [PubMed: 11267681]
20. Hashimoto T, Kato M, Shimomura T, Kitamura N. TMPRSS13, a type II transmembrane serine protease, is inhibited by hepatocyte growth factor activator inhibitor type. 1 and activates pro-hepatocyte growth factor. Febs J. 2010; 277:4888–4900. [PubMed: 20977675]
21. List K, Haudenschild CC, Szabo R, Chen W, Wahl SM, Swaim W, Engelholm LH, Behrendt N, Bugge TH. Matriptase/MT-SP1 is required for postnatal survival, epidermal barrier function, hair follicle development, and thymic homeostasis. Oncogene. 2002; 21:3765–3779. [PubMed: 12032844]
22. Chen Y, Merzdorf C, Paul DL, Goodenough DA. COOH terminus of occludin is required for tight junction barrier function in early Xenopus embryos. J. Biol. Chem. 1997; 138:891–899.
23. Leyvraz C, Charles RP, Rubera I, Guitard M, Rotman S, Breiden B, Sandhoff K, Hummler E. The epidermal barrier function is dependent on the serine protease CAP1/Prss8. J. Cell Biol. 2005; 170:487–496. [PubMed: 16061697]
24. List K, Szabo R, Wertz PW, Segre J, Haudenschild CC, Kim SY, Bugge TH. Loss of proteolytically processed filaggrin caused by epidermal deletion of Matriptase/MT-SP1. J. Cell Biol. 2003; 163:901–910. [PubMed: 14638864]
25. Nagaike K, Kawaguchi M, Takeda N, Fukoshima T, Sawaguchi A, Kohama K, Setoyama M, Kataoka H. Defect of hepatocyte growth factor activator inhibitor type 1/serine protease inhibior, Kunitz type 1 (Hai-1/Spint1) leads to ichthyosis-like condition and abnormal hair development in mice. Am. J. Pathol. 2008; 173:1–12.
26. Szabo R, Kosa P, List K, Bugge TH. Loss of matriptase suppression underlies spint1 mutation-associated ichthyosis and postnatal lethality. Am. J. Pathol. 2009; 174:2015–2022. [PubMed: 19389929]
27. Nemes Z, Steinert PM. Bricks and mortar of the epidermal barrier. Exp. Mol. Med. 1999; 31:5–19. [PubMed: 10231017]
28. Furuse M, Hata M, Furuse K, Yoshida Y, Haratake A, Sugitani Y, Noda T, Kubo A, Tsukita S. Claudin-based tight junctions are crucial for the mammalian epidermal barrier: a lesson from claudin-1-deficient mice. J. Cell Biol. 2002; 156:1099–1111. [PubMed: 11889141]
29. List K, Hobson JP, Molinolo A, Bugge TH. Co-localization of the channel activating protease prostasin/(CAP1/PRSS8) with its candidate activator, matriptase. J. Cell. Physiol. 2007; 213:237–245. [PubMed: 17471493]

30. List K, Szabo R, Molinolo A, Nielsen BS, Bugge TH. Delineation of matriptase protein expression by enzymatic gene trapping suggests diverging roles in barrier function, hair formation, and squamous cell carcinogenesis. Am. J. Pathol. 2006; 168:1513–1525. [PubMed: 16651618]

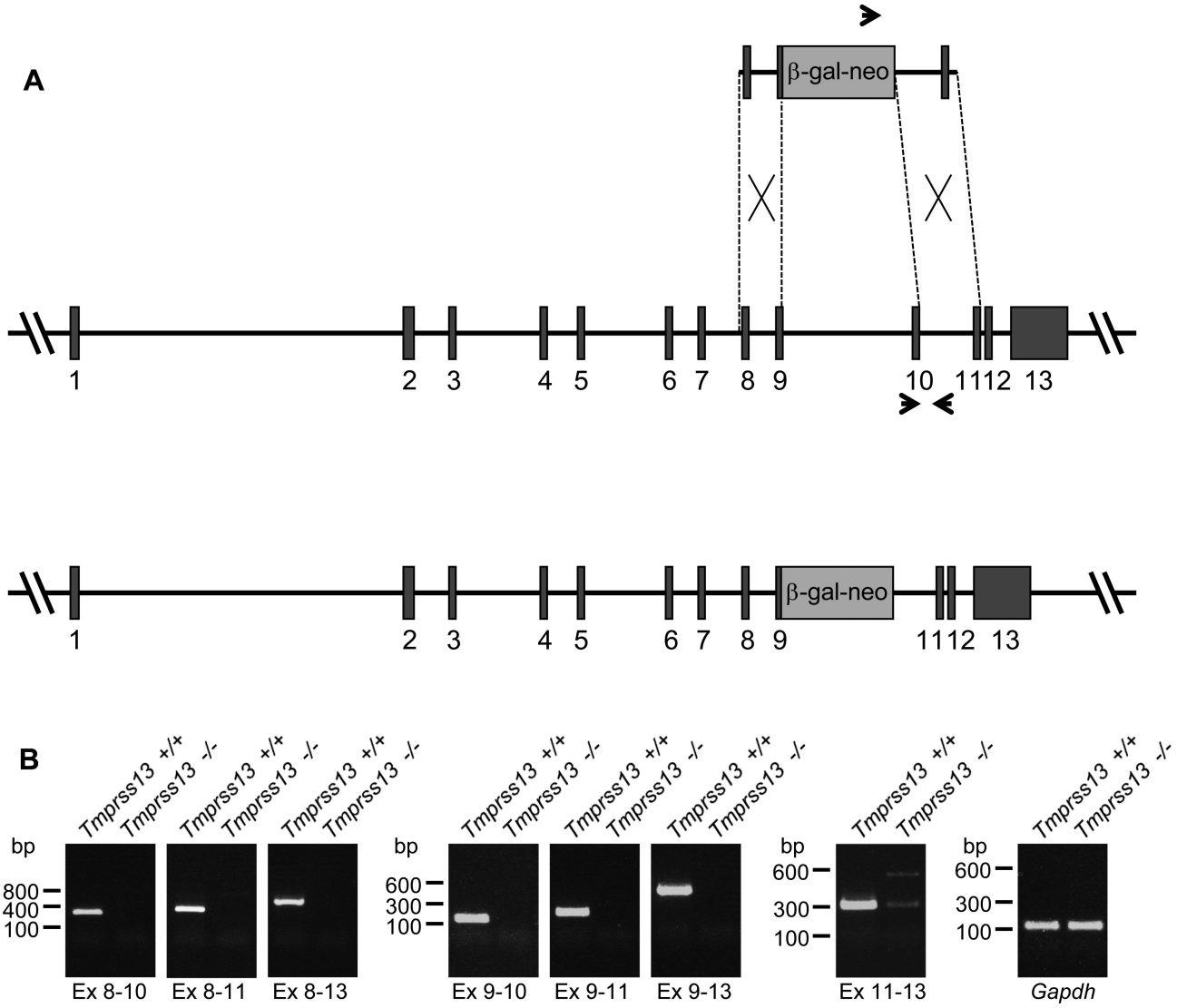

Figure 1. Targeting of the *Tmprss13* gene in mice

(**A**) Structure of targeting vector (top), wildtype *Tmprss13* allele (middle), and targeted *Tmprss13* allele (bottom). Exons are indicated as blue boxes and intron sequences as black lines. The locations of primers used for PCR genotyping of mice are indicated by green arrowheads. Homologous recombination in ES cells replaced a 4 kb region of the *Tmprss13* gene, including the last 92 bp of exon 9 and the entire exon 10, with a β-galactosidase-neomycin resistance fusion gene (orange box) lacking promoter sequences and a methionine initiation codon. The *Tmprss13* deletion includes exon 9 sequences that encode Asp395, which forms part of the catalytic His-Asp-Ser triad. The β-galactosidase-neomycin resistance fusion gene is placed in frame with exon 9 leading to the formation of a tripartite TMPRSS13-β-galactosidaseneomycin fusion protein containing the first 377 amino acids of TMPRSS13. (**B**) Analysis of *Tmprss13* mRNA transcripts in *Tmprss13* targeted mice shows the elimination of exon 10-containing *Tmprss13* mRNA transcripts and absence of alternatively spliced mRNA transcripts containing exons upstream and downstream from the β-galactosidase-neomycin fusion gene. RT-PCR analysis was performed using mRNA

isolated from the skin of pairs of wildtype (left lanes) and *Tmprss13*$^{-/-}$ (right lanes) mice. Specific amplicons are indicated under each panel. Amplification of *Gapdh* mRNA was performed as a positive control. Size markers (bp) are shown on the left.

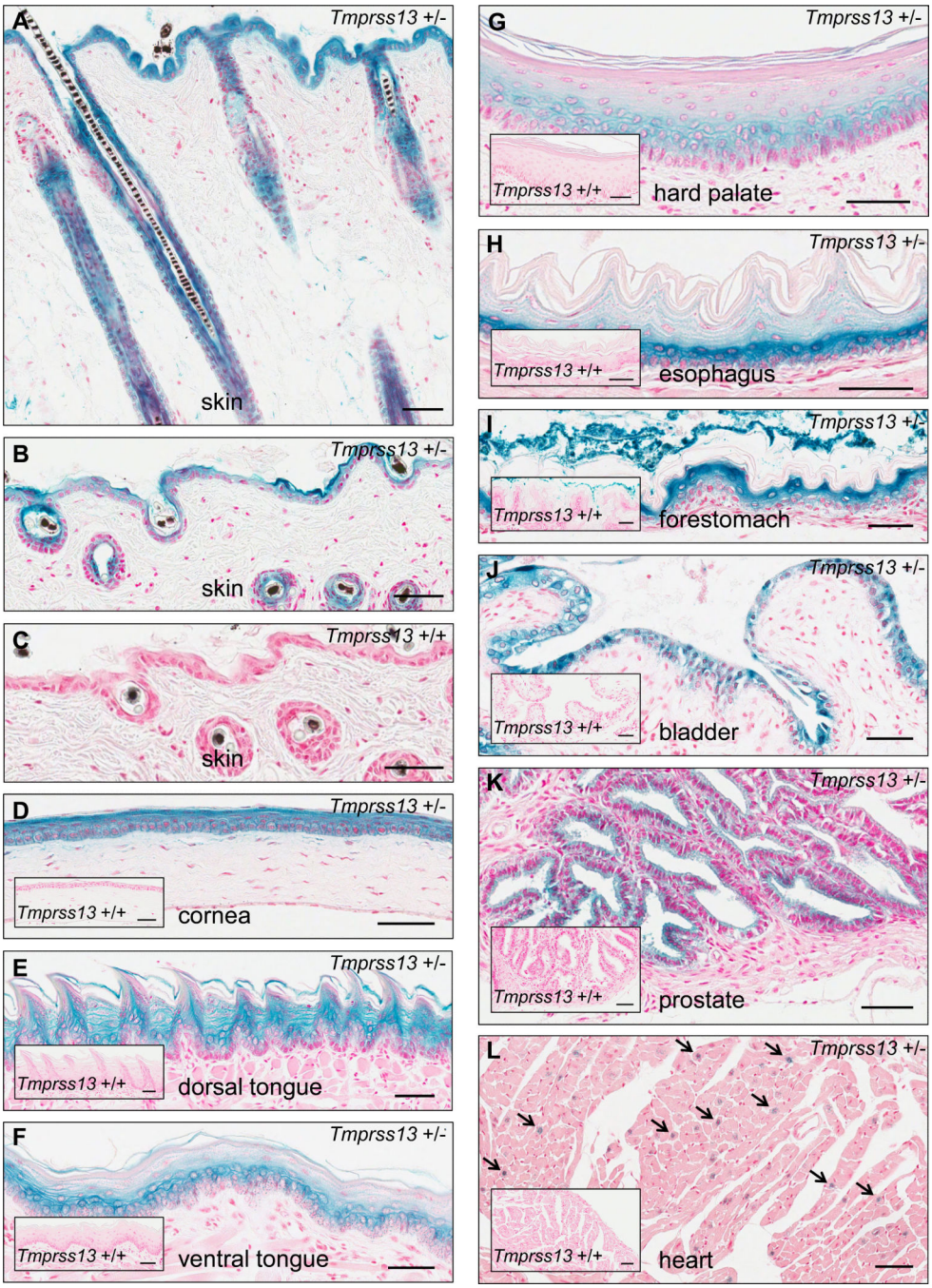

Figure 2. *Tmprss13* is expressed at high levels in stratified squamous and transitional bladder epidermalithelium

(**A** and **B, D-L**) Representative X-gal staining of skin (**A** and **B**), cornea (**D**), dorsal (**E**) and ventral (**F**) tongue, hard palate (**G**), esophagus (**H**), forestomach (**I**), bladder (**J**), prostate (**K**) and heart (**L**) from a young adult Tmprss13$^{+/-}$ mouse and skin from a wildtype littermate (**B**). The skin is sectioned at different angles in **A** and **B** to illustrate the staining of hair follicles. **(C)** X-gal staining of skin from a wildtype littermate mouse as a control for

staining specificity. Inserts in **D-L** show X-gal staining of the same tissue from a wildtype littermate mouse. All sections were counterstained with nuclear fast red. Size bars = 50 μm.

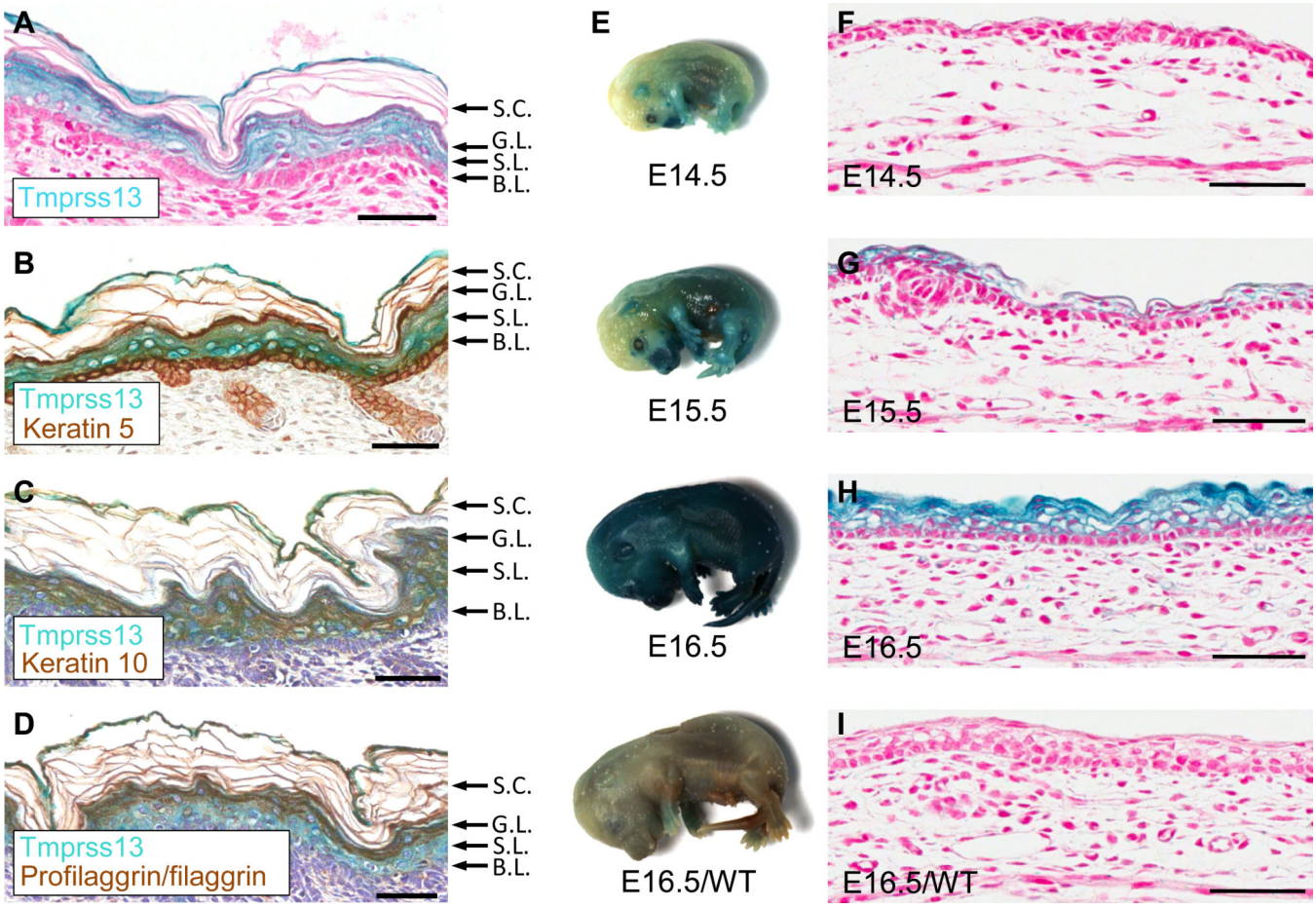

Figure 3. *Tmprss13* is expressed in the suprabasal layers of the interfollicular epidermis and onset of expression correlates with acquisition of epidermal barrier function

(**A-D**) Histological sections of skin from a newborn Tmprss13$^{+/-}$ mouse was X-gal stained and counterstained with Nuclear Fast Red (**A**) or X-gal stained and immunohistochemically co-stained with antibodies against keratin 5 (**B**), keratin 10 (**C**), or profilaggrin/filaggrin (**D**). Sections in **B-D** were counterstained with Mayer's hematoxylin. *Tmprss13* expression is co-localizing with keratin 10 and profilaggrin/filaggrin but not with the basal keratin 5-positive keratinocytes. (**A-D**) The stratum corneum (S.C.), granular layer (G.L.), suprabasal layer (S.L.), and basal layer (B.L.) are indicated with arrows. (**E**) Mouse embryos at E14.5-E16.5 were whole-mount stained with X-gal. Weak *Tmprss13* expression in embryonic surface ectoderm/epidermis was observed already at E14.5 and increased to become intense and uniform at E16.5. An E16.5 littermate wildtype embryo (E16.5/WT) was included as a control for staining specificity. (**F-I**) X-gal stained histological sections of surface ectoderm/epidermis from Tmprss13$^{+/-}$ embryos at E14.5 **(F)**, E15.5 **(G)**, and E16.5 **(H)** and a wildtype littermate embryo at E16.5 **(I).** Sections were counterstained with nuclear fast red. Size bars = 50 μm.

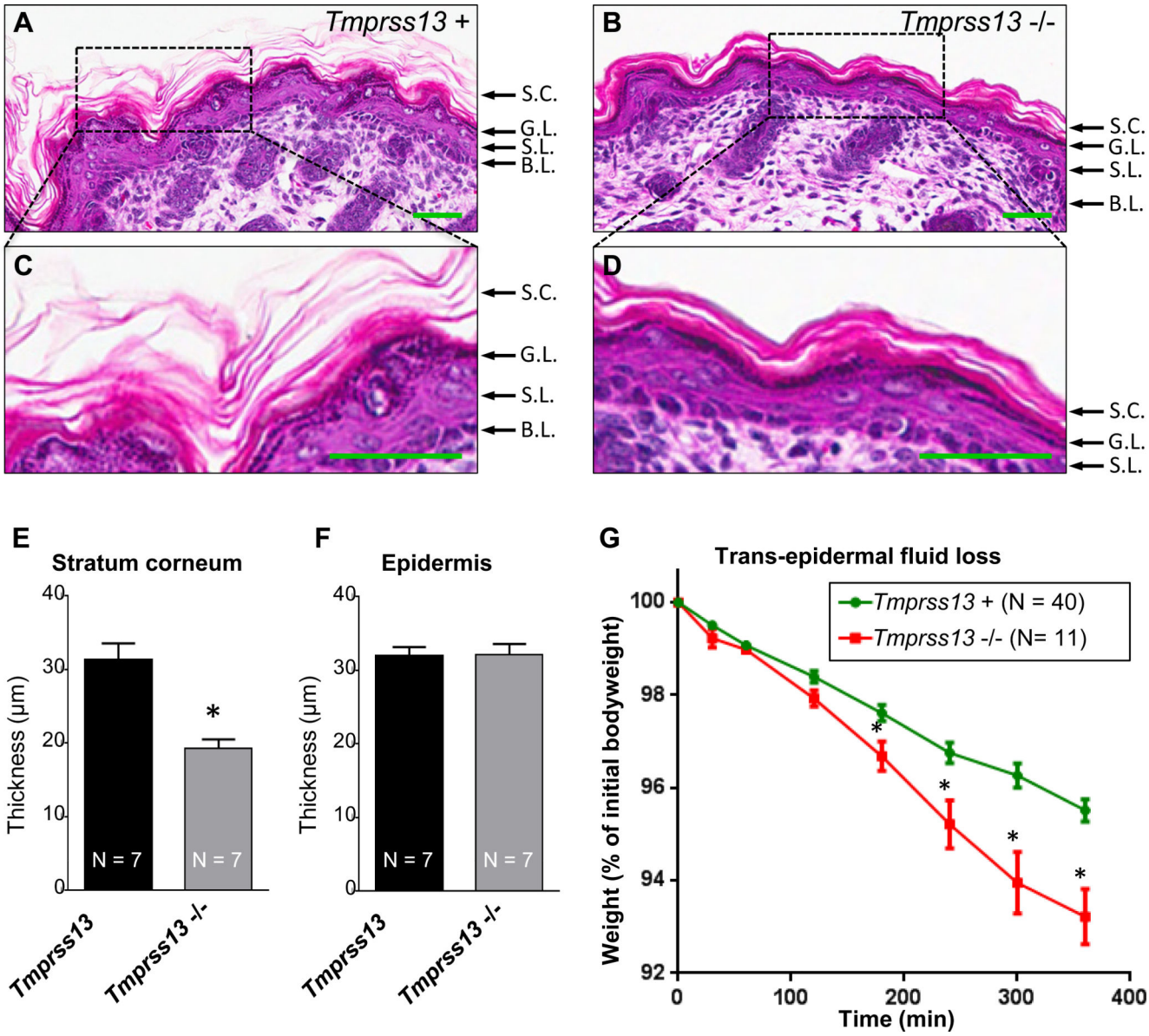

Figure 4. Loss of TMPRSS13 compromises stratum corneum formation and epidermal barrier function

Low (**A** and **B**) and high (**C** and **D**) magnification of H&E stained sections of epidermis from a newborn control mouse (**A** and **C**) and from a littermate *Tmprss13*$^{-/-}$ mouse (**B** and **D**). Note the thinner and more compact appearance of the *Tmprss13*$^{-/-}$ stratum corneum. Size bars = 50 µm. (**A-D**) The stratum corneum (S.C.), granular layer (G.L.), suprabasal layer (S.L.), and basal layer (B.L.) are indicated with arrows. (**E** and **F**) Histomorphometric quantification of the thickness of the stratum corneum (**E**) and the epidermis (excluding the stratum corneum) (**F**) of *Tmprss13*$^{+}$ (black bars, N = 7) and *Tmprss13*$^{-/-}$ (grey bars, N = 7) littermates. **(G)** Trans-epidermal fluid loss from newborn control (N = 40) and Tmprss13$^{-/-}$ (N=11) littermates, as assessed by reduction of body weight as a function of time. Error bars in **C-E** indicate SEM. * $p < 0.05$ (Student's t-test, two-tailed).

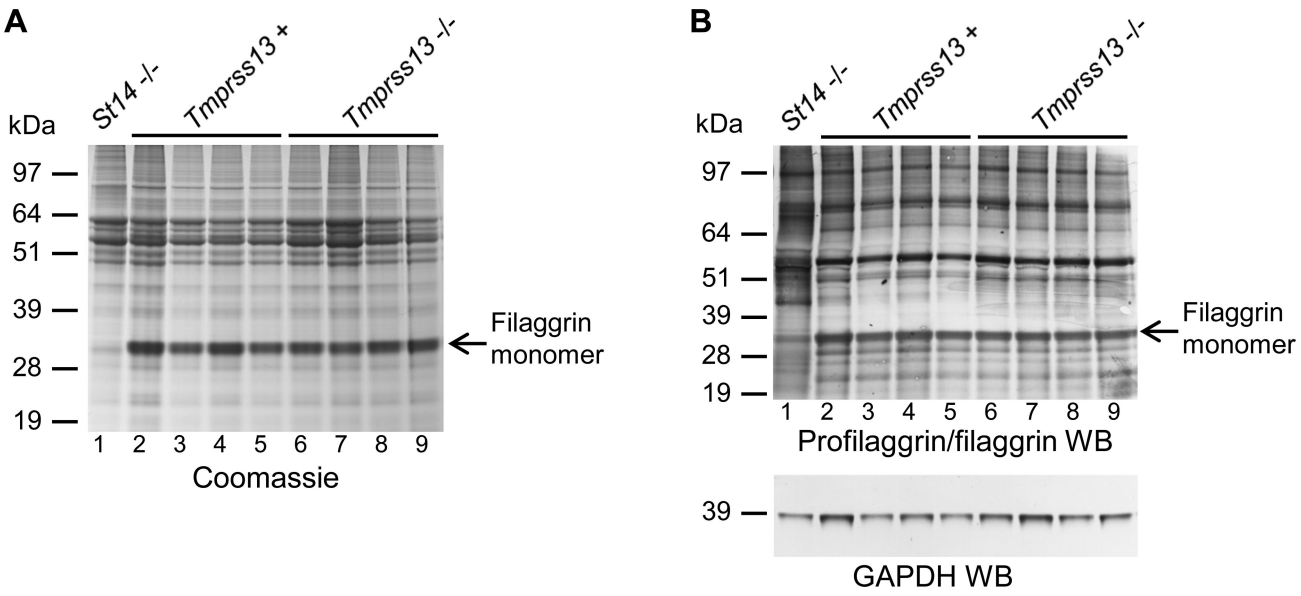

Figure 5. Profilaggrin processing is independent of TMPRSS13

SDS-PAGE and Coomassie staining **(A)** and profilaggrin/filaggrin Western blotting **(B)** of urea extracts from the epidermis of newborn *St14*$^{-/-}$ (lane 1), control (lanes 2-5), and *Tmprss13*$^{-/-}$ (lanes 6-9) mice. The position of the filaggrin monomer is indicated on the right. Positions of molecular weight makers (kDa) are indicated on the left. Filaggrin is absent in matriptase-deficient epidermis, whereas filaggrin levels are unaffected by the absence of TMPRSS13.

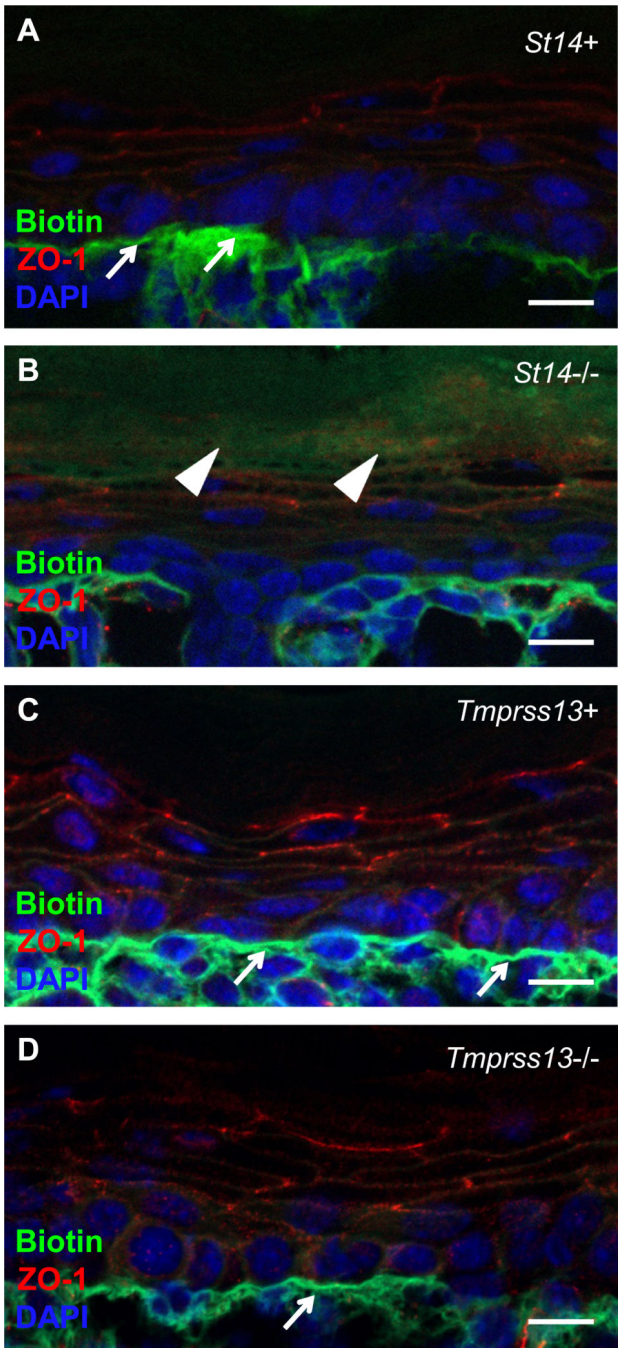

Figure 6. Epidermal tight junctions are functional in TMPRSS13-deficient mice

Newborn *St14*$^{+/+}$ **(A)**, littermate *St14*$^{-/-}$ **(B)**, *Tmprss13*$^{+/+}$ **(C)**, and littermate *Tmprss13*$^{-/-}$ **(D)** mice were injected intradermally with Sulfo-NHS-LC-Biotin (examples with arrows in **A, C** and **D**). After 30 min the skin was excised, sectioned, and stained for biotin (green) and ZO-1 (red). Nuclei (blue) were stained with DAPI. Accumulation of the biotin tracer is observed in the stratum corneum of *St14*$^{-/-}$ (examples with arrowheads in **B**), but not in wildtype or *Tmprss13*$^{-/-}$ stratum corneum (**A, C**, and **D**) in matriptase-deficient epidermis

(**D**). Size bars = 10 μm. A total of 8 *Tmprss13*$^{+/+}$ and 6 littermate *Tmprss13*$^{-/-}$ mice were analyzed with similar results.

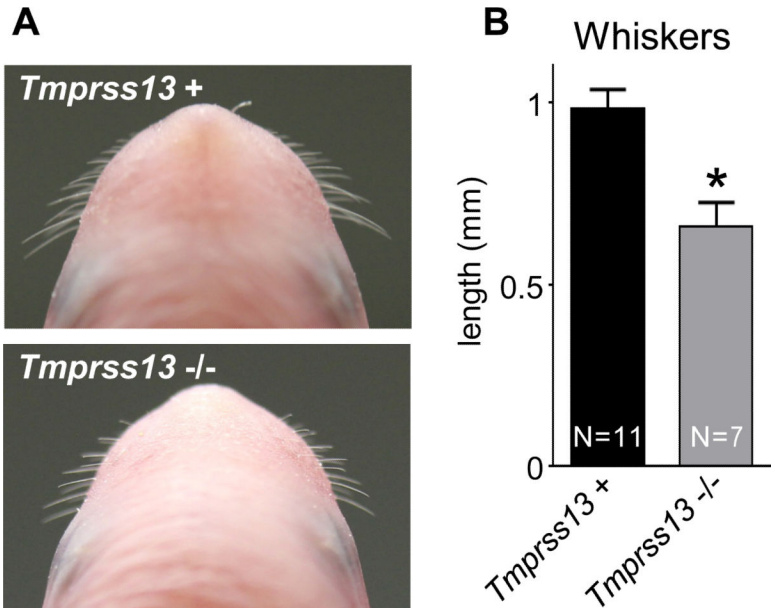

Figure 7. Abnormal whisker development in TMPRSS13-deficient mice

(**A**) Representative appearance of whiskers of newborn control mice (left panel) and littermate *Tmprss*13$^{-/-}$ mice (right panel). (**B**) Quantification of whisker length in newborn mice. The root-to-tip length of the longest whisker of each mouse was determined. The graph shows the average length of whiskers from newborn control mice (n=11, black bar) and from littermate *Tmprss13*$^{-/-}$ mice (n=6, grey bar). Error bars in **B** indicate SD. * $p<0.001$ (Student's t-test, two-tailed).

Table 1

RT-PCR primers.

name	sequence
Tmprss13 exon 8 forward	CTCATCGATGCCCAGTGG
Tmprss13 exon 9 forward	CAACTACACAGATGAACAGG
Tmprss13 exon 10 reverse	CAACAGGTCTCATTGAGGC
Tmprss13 exon 11 forward	GAAGTGCAATGACTACTTGG
Tmprss13 exon 11 reverse	GTTGACCTGAACCTCTCGG
Tmprss13 exon 13 reverse	GGATCTTCATAGCAGTCAGC

Table 2

Summary of the expression of *Tmprss13* in adult mouse tissues based on X-gal staining.

skin	+++
tongue	+++
lip	+++
hard pallate	+++
cornea	+++
bladder	+++
esophagus	++
stomach*	++
prostate	++
intestine	+
heart	+
thymus	+
kidney**	+
testis	(+)
colon	-
liver	-
spleen	-
lung	-
uterus	-
ovary	-
muscle	-

- = no staining. + = weak staining. ++ = medium staining. +++ = strong staining. (+) = weak staining difficult to distinguish from unspecific staining of wildtype tissues.

* Forestomach was positive whereas the glandular part of the stomach was negative.

** Ureter was positive but the remaining part of the kidney was essentially negative.